ACS Partner Journal

CHEMICAL & BIOMEDICAL IMAGING

Editors' Choice

Open Access

pubs.acs.org/ChemBioImaging

Article

Developing Hyperpolarized Butane Gas for Ventilation Lung Imaging

Nuwandi M. Ariyasingha,* Anna Samoilenko, Md Raduanul H. Chowdhury, Shiraz Nantogma, Clementinah Oladun, Jonathan R. Birchall, Tarek Bawardi, Oleg G. Salnikov, Larisa M. Kovtunova, Valerii I. Bukhtiyarov, Zhongjie Shi, Kehuan Luo, Sidhartha Tan, Igor V. Koptyug, Boyd M. Goodson, and Eduard Y. Chekmenev*

Cite This: *Chem. Biomed. Imaging* 2024, 2, 698−710

Read Online

ACCESS | Metrics & More | Article Recommendations | Supporting Information

ABSTRACT: NMR hyperpolarization dramatically improves the detection sensitivity of magnetic resonance through the increase in nuclear spin polarization. Because of the sensitivity increase by several orders of magnitude, additional applications have been unlocked, including imaging of gases in physiologically relevant conditions. Hyperpolarized ^{129}Xe gas recently received FDA approval as the first inhalable gaseous MRI contrast agent for clinical functional lung imaging of a wide range of pulmonary diseases. However, production and utilization of hyperpolarized ^{129}Xe gas faces a number of translational challenges including the high cost and complexity of contrast agent production and imaging using proton-only (i.e., conventional) clinical MRI scanners, which are typically not suited to scan ^{129}Xe nuclei. As a solution to circumvent the translational challenges of hyperpolarized ^{129}Xe, we have recently demonstrated the feasibility of a simple and cheap process for production of proton-hyperpolarized propane gas contrast agent using ultralow-cost disposable production equipment and demonstrated the feasibility of lung ventilation imaging using hyperpolarized propane gas in excised pig lungs. However, previous pilot studies have concluded that the hyperpolarized state of propane gas decays very fast with an exponential decay T_1 constant of ∼0.8 s at 1 bar (physiologically relevant pressure); moreover, the previously reported production rates were too slow for potential clinical utilization. Here, we investigate the feasibility of high-capacity production of hyperpolarized butane gas via heterogeneous parahydrogen-induced polarization using Rh nanoparticle-based catalyst utilizing butene gas as a precursor for parahydrogen pairwise addition. We demonstrate a remarkable result: the lifetime of the hyperpolarized state can be nearly doubled compared to that of propane (T_1 of ∼1.6 s and long-lived spin-state T_S of ∼3.8 s at clinically relevant 1 bar pressure). Moreover, we demonstrate a production speed of up to 0.7 standard liters of hyperpolarized gas per second. These two synergistic developments pave the way to biomedical utilization of *proton*-hyperpolarized gas media for ventilation imaging. Indeed, here we demonstrate the feasibility of phantom imaging of hyperpolarized butane gas in Tedlar bags and also the feasibility of subsecond 2D ventilation gas imaging in excised rabbit lungs with 1.6 × 1.6 mm^2 in-plane resolution using a clinical MRI scanner. The demonstrated results have the potential to revolutionize functional pulmonary imaging with a simple and inexpensive on-demand production of *proton*-hyperpolarized gas contrast media, followed by visualization on virtually any MRI scanner, including emerging bedside low-field MRI scanner technology.

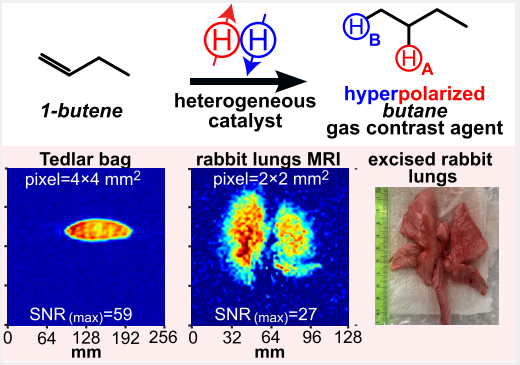

KEYWORDS: *NMR hyperpolarization, propane, butane, pulmonary imaging, ventilation MRI, rabbit, lungs*

INTRODUCTION

NMR is a widely utilized spectroscopic technique that relies on energy transitions between nuclear spin Zeeman energy levels. The NMR signal is proportional to the population difference between these energy levels—the nuclear spin polarization (P)—i.e., the degree of alignment of the nuclear spin ensemble with the applied magnetic field.[1,2] P is on the order of 10^{-6}–10^{-5} for clinically relevant magnetic fields and body temperature, causing NMR and MRI to suffer a distinct sensitivity disadvantage compared to many other spectroscopic and imaging techniques.[1] This low sensitivity limits the spatio-temporal resolution of MRI *in vivo*; as a result, only highly concentrated species such as tissue fat and water can be imaged

Received: May 3, 2024
Revised: July 3, 2024
Accepted: July 5, 2024
Published: July 25, 2024

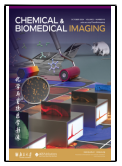

with good resolution. Several hyperpolarization technologies have been developed to increase P to the order of unity, i.e., several orders of magnitude above the thermal equilibrium level.[1,3−7] This massive P increase leads to corresponding gains in the observed NMR signal and enables detection of dilute biologically relevant molecules that can be administered by injection or inhalation.[4,8−12] These low-concentration species can effectively be utilized as hyperpolarized (HP) MRI contrast agents *in vivo*.[10,12−14]

One group of applications employ HP ^{129}Xe gas as an inhalable HP contrast agent for functional pulmonary imaging, which plays an important role for diagnosis and management of a wide range of lung diseases, including COPD, asthma, Idiopathic Pulmonary Fibrosis (IPF), etc.[8,15−21] Modern commonly used pulmonary imaging techniques include Chest X-ray (CRX), Computed Tomography (CT) scanning, single-photon emission computed tomography (SPECT) with ^{133}Xe imaging,[22] and conventional MRI.[15,23−25] However, since CT, CRX, and MRI image tissue density, the functional information about lung ventilation is obtained indirectly via surrogate metrics, e.g., as beam attenuation in CT. HP ^{129}Xe contrast agent gas shines with a distinct advantage over other imaging techniques as it follows the same path as inhaled air, and thus, HP ^{129}Xe MRI allows one to visualize regional lung ventilation.[26−30] Although ^{133}Xe SPECT in principle reports on similar functionality as HP ^{129}Xe, ^{133}Xe is radioactive and provides only low-resolution 2D projection images.[15,22]

HP ^{129}Xe gas has been successfully employed as a HP gas contrast agent for lung imaging in both preclinical and clinical settings.[8,15−17,19,21,31−36] In December 2022, HP ^{129}Xe received FDA approval as the first inhalable HP gas contrast agent for functional lung imaging of adults and pediatric patients above 12 years. HP ^{129}Xe is produced via Spin Exchange Optical Pumping (SEOP) on a clinical scale.[17,37] This hyperpolarization technique requires hardware that has a relatively high cost (~$0.5−0.9 M) and low production throughput (1−3 doses per hour). Besides the equipment and operational costs, clinical utilization requires enriched gas with an over 80% ^{129}Xe fraction that costs over $300 per liter, representing a human dose.[15] The bigger problem, however, is that conventional MRI scanners are designed for imaging of protons of fat and water and cannot be readily employed for MRI scanning of HP ^{129}Xe nuclei; indeed, a multinuclear scanner upgrade is required to enable ^{129}Xe scanning, embodying additional substantial capital investment of $0.2−0.6M. Furthermore, such upgrades are limited to selected vendor platforms, i.e., not universally available on all MRI scanners.

Alternative approaches to ^{129}Xe HP gas contrast media are greatly desired. One such approach is the utilization of Parahydrogen-Induced Polarization (PHIP).[38,39] PHIP employs parahydrogen (p-H_2) gas as a cheap source of hyperpolarization.[38,39] The symmetry of the otherwise-NMR-silent p-H_2 singlet state can be broken when it is added to an unsaturated precursor molecule in a pairwise manner and the nascent H atoms end up in magnetically inequivalent positions in the product molecule.[38−40] These p-H_2-derived protons can gain large P in the HP product molecule.[38−40] For example, gas-phase pairwise p-H_2 addition to propene over specialized heterogeneous catalysts can yield HP propane gas,[40−42] which can be visualized via MRI.[43,44] This hyperpolarization approach has a substantially lower instrumentation and operating cost compared to SEOP.[45,46] Indeed, we have recently demonstrated production of HP propane gas contrast agent using an ultralow-cost hand-held disposable hyperpolarizer capable of producing 0.15 standard liters per second (sLs) of HP gas and demonstrated the utility of this device for pilot imaging of excised pig lungs with 4 × 4 mm^2 in-plane spatial resolution.[47] Propane (also known as food additive E944) in its nonhyperpolarized form is regulated by the FDA, and propane is generally recognized as safe (GRAS) due to its low toxicity. HP propane gas can be imaged on virtually any clinical MRI scanner.[47] The key limitation of HP propane gas as an inhalable MRI contrast agent is the relatively short lifetime of its HP state.[48,49] Indeed, the exponential decay time constant (T_1) for HP propane is only 0.79 ± 0.02 s at physiologically relevant conditions (1 bar pressure, Figure S2); here, T_1 is limited by the molecular spin-rotation relaxation mechanism.[50,51] This value compares unfavorably to the corresponding HP ^{129}Xe T_1 of ~20 s (unlike with propane, the ^{129}Xe T_1 in pulmonary spaces is limited primarily by the presence of paramagnetic O_2).[15] Thus, proton-hyperpolarized HP gas contrast agents with longer T_1 are greatly desired[52,53] to retain the HP state during the lung ventilation MRI scan.

Here, we investigate the feasibility of heterogeneous (HET) PHIP hyperpolarization of butane gas using 1-butene and 2-butene as gaseous precursors for pairwise p-H_2 addition (Scheme 1). We demonstrate that the T_1 of HP butane is nearly doubled to 1.55 ± 0.05 s compared to that of HP propane at the physiologically relevant pressure of 1 bar, thus potentially mitigating the key propane limitation, Figure S2. We also demonstrate an ultrahigh-flow (a.k.a. high-capacity) production rate of HP butane gas of up to 0.7 sLs (approximately 4−5 times faster than the previous record using HP propane[47]). The produced HP gas bolus was injected into a Tedlar bag and visualized via subsecond 2D MRI using a 0.35 T clinical MRI scanner. Feasibility of high-resolution lung ventilation imaging is demonstrated in excised rabbit lungs with a spatial resolution as good as 1.6 × 1.6 mm^2 (2D pixel size) using this clinical MRI scanner. We also demonstrate that the lifetime of HP butane gas can be further prolonged through the creation of long-lived spin states (LLSSs) that are present at 0.0475 T: indeed, T_S of up to 3.8 s is demonstrated at 1 bar pressure. Remarkably, the LLSS lifetime is longer when employing the 1-butene precursor versus the 2-butene precursor, which is rationalized by overpopulation of different spin states in the corresponding reaction products. Since butane gas is GRAS according to FDA, and it is also employed as a food additive E943a (and thus is relatively nontoxic), the results reported here bode well for future utilization of HP butane as a next-generation HP contrast agent gas for functional pulmonary imaging.

MATERIALS AND METHODS

Production of Hyperpolarized Hydrocarbon Gases for Spectroscopic Studies at 1.4 and 0.0475 T

For heterogeneous pairwise p-H_2 addition to 1-butene, 2-butene, and propene, a 1:1 gas mixture of a corresponding substrate−precursor (propene (>99%, Airgas PP CP35 GR2.0), 1-butene (>99%, Sigma P/N 295051), or 2-butene (>99%, mixture of cis- and trans-isomers, Sigma P/N 363359)) and p-H_2 was prepared in a 0.7 L aluminum storage tank equipped with a brass gas pressure regulator. All experiments employed p-H_2 gas with 95−98% para-fraction produced from ultrapure H_2 (>99.999%, Airgas).[56] The storage tank was first flushed with the corresponding precursor gas and then loaded with the pressurized precursor to a desired pressure. Finally, p-H_2 gas was

https://doi.org/10.1021/cbmi.4c00041
Chem. Biomed. Imaging 2024, 2, 698−710

Scheme 1. Schematics of Pairwise p-H_2 Addition to Unsaturated Substrates[a]

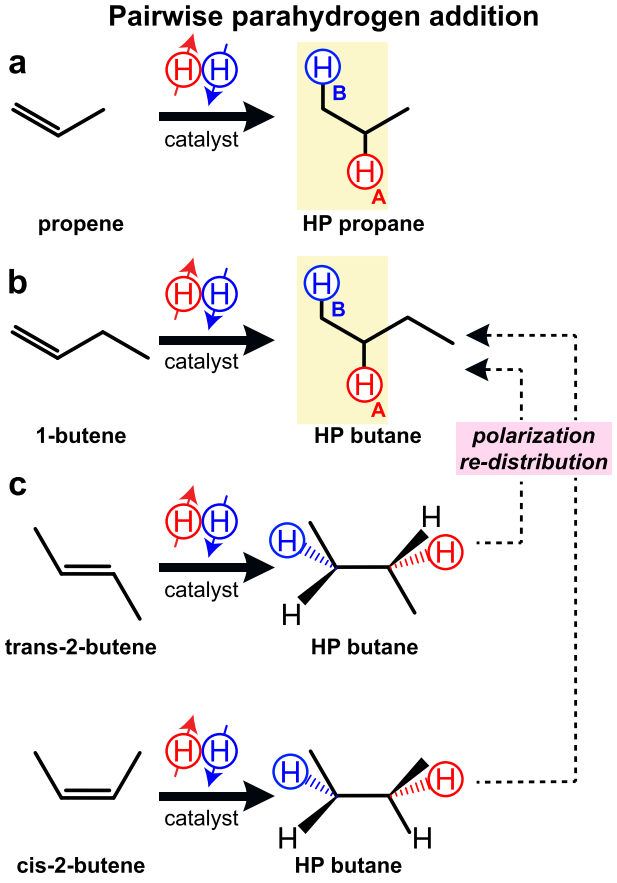

[a](a) Propene, resulting in HP propane; (b) 1-butene, resulting in HP butane; (c) a mixture of trans-2-butene and cis-2-butene, resulting in HP butane. Note that here the reactions are performed under ALTADENA conditions[54] and polarization redistribution[55] may occur resulting in hyperpolarization of protons beyond those derived from p-H_2. Note that different spin states can be overpopulated in the products of p-H_2 addition to 2-butenes versus that of 1-butene, which may not be reflected in this simplified schematic. The H_A and H_B notations refer to the appearance of spectral lines in high-field NMR spectra.

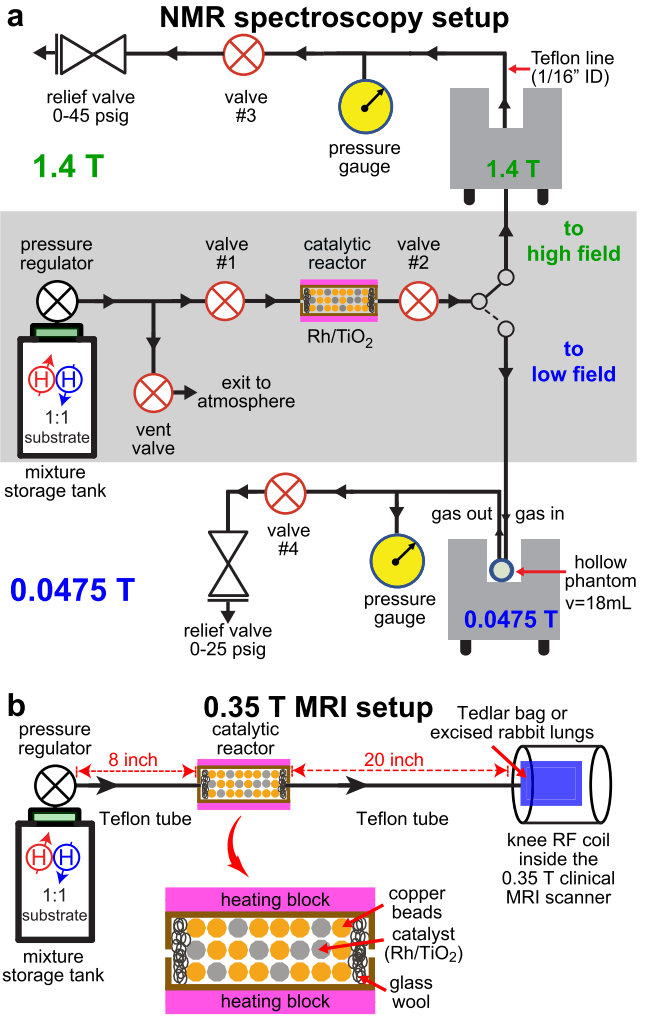

Figure 1. (a) Experimental setup for heterogeneous pairwise p-H_2 addition to unsaturated substrate molecules (propene, 1-butene, or 2-butene). The storage gas tank contained a 1:1 gas mixture of p-H_2 and the unsaturated precursor that is directed through the reactor (heated to 150 °C) using manual valves. HP product gas exits the reactor, and it is directed to the NMR detector (with the gas being detected inside a 1/16-in.-ID Teflon line at 1.4 T or inside a hollow plastic spherical phantom when using the 0.0475 T magnet). The estimated flow rate of the HP gas was 6−8 sLm. (b) MRI experimental polarizer setup used for clinical-scale imaging. A portable gas-mixing storage tank is connected to the high-flow catalytic reactor (estimated flow rate is 30−40 sLm). The HP gas exits the reactor and inflates the Tedlar bag situated in the knee RF coil of a 0.35 T clinical MRI scanner (see the main text describing the setup modification for HP gas injection inside the excised rabbit lungs). Parahydrogen addition was performed at the Earth's magnetic field.

added to create a 1:1 mixture with the corresponding unsaturated precursor. The final pressures of the gas mixtures were set to 160 psig for the propene:p-H_2 mixture and 70−80 psig for the butene:p-H_2 mixtures, respectively. Within 1 h of filling of the tank, hyperpolarization reactions were performed at the Earth's magnetic field using the portable hyperpolarizer setup, Figure 1a. All gas-handling lines in the hyperpolarizer setup are made of 1/8-in. OD (1/16-in. ID) Teflon tubing (McMaster-Carr, P/N 5239K24). A reactant gas mixture was directed through the catalytic reactor filled with Rh/TiO_2 (0.9 wt % Rh, solid-phase catalyst,[57] heated to 150 °C) by opening the valves #1 and #2 and either valve #3 or #4, Figure 1a. The catalytic reactor employed the loading of 0.2 g of catalyst mixed with copper beads and placed in 1/4-in. OD copper tubing (McMaster-Carr, P/N 5174K21) as described previously.[47] As the gas mixture flows through the catalytic reactor, pairwise p-H_2 addition to the unsaturated hydrocarbon occurs, and the produced HP gas is directed into the NMR spectrometer (1.4 or 0.0475 T) for detection. The overall pressure in the detection volume of the NMR instrument was controlled by a relief valve set to a desired pressure in the range of 0 to 45 psi overpressure. The gas flow was 6−8 standard liters per minute (sLm) of the final HP product gas, as measured by a water displacement test. The actual pressure reading was performed using a pressure gauge, Figure 1a.

We used a 1.4 T benchtop NMR spectrometer (Nanalysis NMR Pro 60) and a low-field 0.0475 T dual-channel Kea2 NMR spectrometer (Magritek, New Zealand) to study the spin relaxation of the produced HP gases. In 1.4 T studies, the Teflon tubing containing the produced HP gas was directed through the bore of the 1.4 T spectrometer to detect ^1H NMR spectra of the HP gas inside the Teflon line, Figure 1a. The 1.4 T detection sequence was programmed to run a set of 64 back-to-back repeat runs (using 15° RF excitation pulses, every 0.5 s) in a pseudo-2D fashion, Scheme 2a.[47] The NMR acquisition was initiated approximately 1−2 s before the gas mixture was directed into the reactor for hyperpolarization to

https://doi.org/10.1021/cbmi.4c00041
Chem. Biomed. Imaging 2024, 2, 698−710

Scheme 2. Schematic Diagram of the Pulse Sequences Used for the Detection of HP Gas[a]

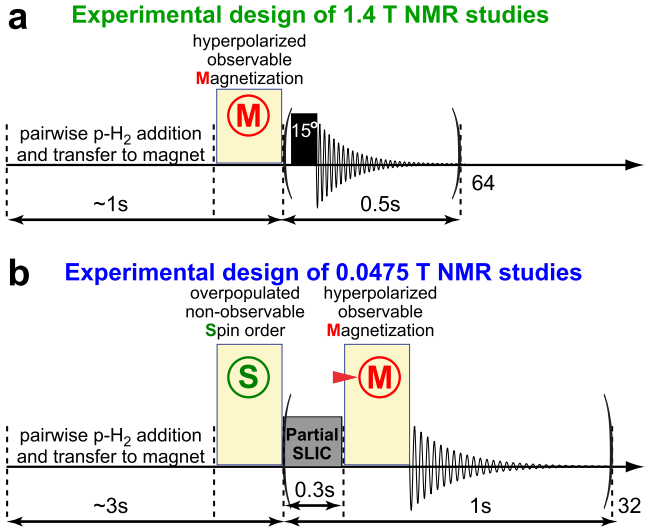

[a](a) In the weakly spin−spin coupled regime, i.e., high field of 1.4 T for detecting H_A and H_B magnetization, and (b) in the strongly spin−spin coupled regime, i.e., low field of 0.0475 T for conversion of singlet spin states into observable magnetization using partial SLIC. Nonobservable singlet spin order and observable magnetization states are used as simplified notations of the overpopulated states of H_A and H_B before and after the SLIC pulse.

ensure the acquisition was active before the hyperpolarization experiment was initiated. After ∼2 s of continuous gas flow, the gas stream was terminated by closing the valves #2 and #3, while the NMR data acquisition of the stopped HP gas was performed to capture the signal decay due to T_1 relaxation.[47] Following the complete return of the gas to a thermal equilibrium state, a thermally polarized spectrum (with known polarization) of the produced gas was acquired using the same acquisition parameters (except for the number of scans); this spectrum was used for signal referencing in polarization enhancement computations (e.g., spectra shown in Figure S1d,h,l). Additionally, an NMR spectrum of thermally polarized product gas was recorded using the same acquisition parameters except for the pulse angle (90° vs 15°) and 64 averages recorded every 5 s to obtain a better signal-to-noise ratio (SNR) to detect any unreacted unsaturated precursor substrate—allowing the reaction chemical conversion to be assessed (Figure S1c,g,k). The recorded NMR signals were used to calculate the signal enhancements of the HP gases and the monoexponential relaxation decay constants using custom MATLAB code (Supporting Information, SI). The depolarizing effect of 15° excitation RF pulses was not taken into account when fitting the decay of the HP state for T_1 measurement (therefore, the presented value may be somewhat underestimated). The reason the depolarizing effect of the excitation RF pulses was not taken into account is because, if the residual gas motion exists (due to minor residual gas flow due to residual speed of the gas or due to gas temperature changes), a nonirradiated sample may potentially displace the partially depolarized sample inside the RF coil: as a result, this compensation approach may lead to an overestimation of the T_1 values. For the pressure-dependent studies in this work, the pressure was varied by selecting the relief valve set to the desired overpressure.

For the 0.0475 T studies, the experiments were performed by using the same overall strategy as that used at 1.4 T, with the following differences. The HP gas product was directed to fill an 18 mL hollow plastic sphere situated inside the radio frequency (RF) probe[58] placed inside the magnet bore of the 0.0475 T NMR spectrometer, and the NMR signal was recorded from the entire plastic sphere filled with the HP gas. The HP gas flow was performed for 3−4 s to displace the unpolarized gas with fresh HP gas. No signal referencing was performed because spectral characterization employed "partial" spin-lock induced crossing (SLIC[59]) pulse[53,60] ("partial" SLIC performs partial transformation of the "singlet" spin state to an observable magnetization, and therefore, polarization quantification is challenging); moreover, NMR signal from the thermally polarized sample did not yield sufficient SNR for quantification. Following the cessation of gas flow using valves #2 and #4 (Figure 1a), a pseudo-2D acquisition was performed using a partial SLIC pulse every second, Scheme 2b—a series of 32 spectral scans of "partial" SLIC-induced NMR signals was performed on a single HP gas refill of the spherical phantom in order to measure signal loss due to the monoexponential decay of long-lived spin states (T_S).

High-Capacity Production of Hyperpolarized Butane and Propane Gases and Subsecond Imaging of Tedlar Bag Phantoms Using 0.35 T MRI

All phantom imaging studies were performed using a 0.35 T clinical MRI scanner (Pica, Time Medical). The HP gases were prepared in the same overall fashion as described in the spectroscopic studies above. For HP butane gas production, the mixing tank was evacuated using a vacuum pump (to 10^{-4} bar for 10 min) and was then loaded with butene gas to approximately 45 psi total pressure. Next, p-H_2 was added (45−50 psi), resulting in the total gas pressure of 90−95 psi. Finally, the mixing tank was placed in the oven at 60 °C for 10−12 min immediately before HP butane production to prevent any butene condensation in the gas lines in the MRI scanner suite. The catalyst-containing reactor was modified to enable a substantially higher gas flow. The exit port of the gas regulator (Figure 1b) was modified to accommodate a connection with 1/4-in. OD (3/16 in. ID, McMaster-Carr, P/N 5239K12), which was connected to the modified reactor. The high-flow reactor was made of a 2.5-in. long brass nipple fitting tube with 1/4-in. NPT male connections (McMaster-Carr, P/N 4568K134), which were capped with 1/4-in. NPT-to-barb tubing fitting connections (McMaster-Carr, P/N 5346K42) on both ends. The catalytic reactor was filled with 0.4 g of Rh/TiO_2 catalyst (0.9 wt % Rh[57]) and 8 g of granulated copper beads (for enhanced heat dissipation of the exothermic hydrogenation reaction) and capped with glass wool on both ends (to prevent catalyst particles from leaving the reactor). The barbed ends of the reactor were fitted directly onto the 1/4-in. OD Teflon tubing using a heat gun. One end of the Teflon tubing was connected to the gas-mixing tank, while the other end was connected to a Tedlar bag (7 × 7-in.^{2}, one-liter capacity, Jensen Inert Products, P/N GST381S-0707TJO) via nonmagnetic push-to-connect fittings, Figure 1b. This reactor design enables HP gas flow rates of 30−40 sLm (measured by a water displacement test). The Tedlar bag was situated inside the knee RF detection coil within the 0.35 T MRI scanner. The HP gas flow rate was increased by 4−6-fold versus our previously developed reactor design using 1/4-in. copper tubing,[45,47] enabling fast inflation (in ∼1 s) of the Tedlar bag. The following imaging parameters were used for phantom studies: gradient echo (GRE) sequence, spectral width (SW) of 10.42 kHz, 5.0 cm slice thickness, 256 × 256 mm^2 field of view (FOV), slice-selective RF pulse of 30°, and 64 × 64 imaging matrix. The imaging sequence was prepared to run 16 repeats in a loop in order to scan the same slice over a 15 s-long duration, yielding 0.97 s temporal resolution. Once the MRI sequence was initiated, HP gas was injected into the Tedlar bag after 2 s of sequence run time. Upon partial bag inflation (typical estimated injected volume of 0.5−0.8 standard liters in 1 s), the tank valve was closed, while image acquisition continued. Typically, image #4 of the sequence yielded the highest SNR of the stopped HP gas in the Tedlar bag. The subsequent repeat scans revealed HP gas depolarization due to the effect of the excitation RF pulses and the HP state decay. No signal from the gas in the Tedlar bag was detected in the last scan (see the SI for more details).

https://doi.org/10.1021/cbmi.4c00041
Chem. Biomed. Imaging 2024, 2, 698−710

Pilot *Ex Vivo* Lung Ventilation MRI at 0.35 T Using HP Butane Gas Contrast Agent

Excised rabbit lungs used for these imaging studies were obtained from other unrelated IACUC-approved studies from the Division of Laboratory Animal Resources at Wayne State University, immediately after the rabbits were euthanized under other unrelated IACUC-approved studies.[61−63] Gas mixture preparation for HET-PHIP hyperpolarization was performed identically to that described in the phantom MRI studies above. The major difference of the experimental setup to that in Figure 1b is that the HET-PHIP reactor employed for spectroscopic studies (with 6−8 sLm flow rate) was used instead of the high-flow reactor employed for the phantom studies because excised rabbit lungs are substantially smaller than a 1 L Tedlar bag and, therefore, would not be able to accommodate 0.8 L of produced HP gas. Thus, the utility of a slower-flow reactor was rationalized by the comparatively smaller-size rabbit lungs. HP butane gas (produced using 1-butene as a precursor) was delivered into the excised lungs via 1/8-in. OD Teflon tubing (similarly to the spectroscopic studies) with the tubing end adapted using a plastic fitting and rubber band to connect to the trachea. A manual nonmagnetic plastic valve was additionally inserted between the reactor and the rabbit lungs to prevent the back flow of butane gas from the rabbit lungs. The 2D GRE images were recorded similarly to those employed for Tedlar bag imaging studies discussed above, with two minor modifications: (1) the HP gas injection was performed immediately after acquisition of scan #4 (which revealed the noninflated thermally polarized lung tissue) after the detection pulse sequence was started (the gas inflation lasted approximately 1 s and delivered an estimated volume of 0.15 sL); (2) FOV was reduced to 128 × 128 mm^2 (main text) or 100 × 100 mm^2 (Figure S14), yielding in-plane spatial resolutions of 2 × 2 mm^2 and 1.6 × 1.6 mm^2, respectively. Images of axial and coronal projections were recorded with the same imaging parameters by using different HP butane gas injections.

■ RESULTS AND DISCUSSION

Hyperpolarized Gas NMR Spectroscopy, Signal Enhancement, and T_1 Relaxation Dynamics at 1.4 T

^{1}H NMR spectroscopic detection of HP butane (produced from 1-butene and 2-butene precursors) revealed the presence of two HP NMR resonances with 180° phase shift (Figure 2a,d, respectively) with an overall similar pattern to that of HP propane shown in Figure 2g. The NMR spectra of HP gases exhibit classic ALTADENA[54] signal patterns, which can be readily assigned to positively polarized H_A methylene and negatively polarized H_B methyl proton resonances for HP propane obtained via pairwise p-H_2 addition to propene (Figure 2g) and for HP butane obtained via pairwise p-H_2 addition to 1-butene (Figure 2a). However, the pairwise addition of p-H_2 to 2-butene (regardless of cis- or trans-configuration present in the precursor mixture, Scheme 1c) implies addition of both nascent p-H_2 derived protons in methylene positions. As a result, H_A and H_B become equivalent chemically but not magnetically. In such a case, both the incoming protons (H_A and H_B) and the protons that lift their magnetic equivalence (in this case, those of the two methyl groups) are expected to show NMR signal enhancement, in agreement with the experimental observation of HP resonances in Figure 2d. Given this experimental observation, Scheme 1c reflects that polarization redistribution may indeed overpopulate many other spin states in butane molecules besides those initially created by the nascent p-H_2 protons.

As described in the Materials and Methods, the HP gas was stopped during the pseudo-2D experiment, where the magnetization is sampled every 0.5 s using a 15° excitation

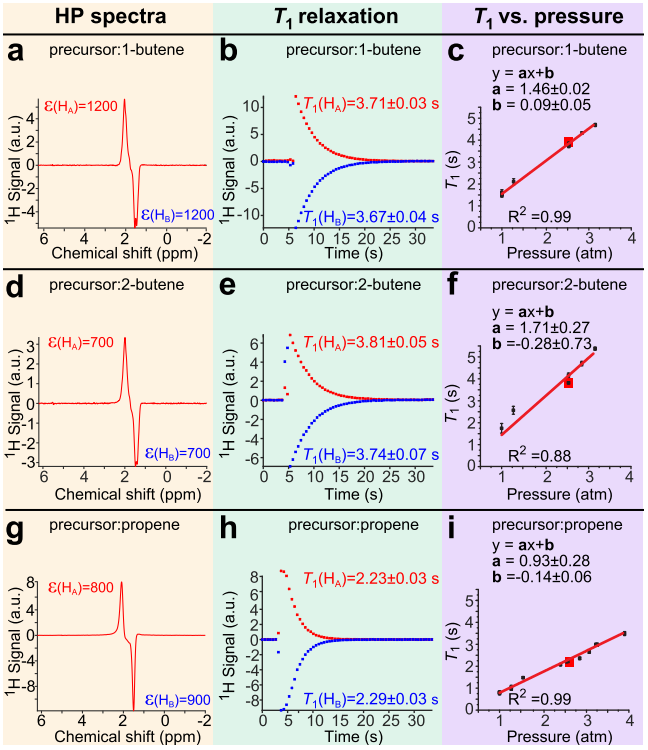

Figure 2. NMR spectroscopy and relaxation dynamics of HP gas at 1.4 T and 2.5 bar pressure (except for panels c, f, and i, where variable pressure was employed). (a) ^{1}H NMR spectrum of HP butane gas produced from 1-butene. (b) T_1 relaxation decay of H_A and H_B protons of HP butane produced from 1-butene. (c) Pressure dependence of T_1 (H_A) of HP butane gas produced from 1-butene. (d) ^{1}H NMR spectrum of HP butane gas produced from 2-butene. (e) T_1 relaxation decay of H_A and H_B protons of HP butane produced from 2-butene. (f) Pressure dependence of T_1 (H_A) of HP butane gas produced from 2-butene. (g) ^{1}H NMR spectrum of HP propane gas. (h) T_1 relaxation decay of H_A and H_B protons in HP propane gas. (i) Pressure dependence of T_1 (H_A) in HP propane gas. Yellow, green, and purple color shading is used to guide the eye. Respective signal enhancements for H_A and H_B protons are given in red and blue for visual clarity. The NMR spectra and decay plots are shown for pressure values denoted by the corresponding red boxes in panels c, f, and i.

pulse. Before the HP gas is stopped, the high gas velocity leads to substantial line broadening—effectively nearly completely canceling the two 180°-phase shifted H_A and H_B resonances during high gas flow.[47] Once the HP gas was fully stopped, both H_A and H_B lines were clearly detected, e.g., Figure 2a, and the stopped HP gas underwent T_1 decay, which was monitored by our pseudo-2D experiment. The intensities of the H_A and H_B resonances were plotted versus time, revealing T_1 decay of the HP state, Figure 2b,e,h. The highest signal enhancement values (ε) were observed in the first NMR acquisition of the stopped HP gas, and these values are reported in Figure 2a,d,g.

Signal enhancements of the H_A and H_B resonances of each HP gas were calculated by taking the ratio of the integrated signal intensities of the HP proton peaks versus the integrated signal intensity of the thermally polarized gas using the same detection parameters, Figure S1 (see the SI for details). The signal enhancement values for H_A and H_B sites reveal overall the same polarization values for HP propane and HP butane (produced from 1-butene) ranging from 800 to 1200, Figure 2g,a, respectively. Signal enhancement values were lower for

https://doi.org/10.1021/cbmi.4c00041
Chem. Biomed. Imaging 2024, 2, 698−710

HP butane originating from 2-butene: $\varepsilon(H_A) = 700$, Figure 2d. These somewhat lower apparent ε values can be potentially explained by the polarization redistribution that overpopulated H_A and H_B differently in the case of butene-2 precursor (Figure S15), although the lower pairwise efficiency of the p-H_2 addition to 2-butene (versus 1-butene) cannot be ruled out in our experiments. The chemical conversion was found to be near 100% for all precursors at all pressure values studied (Figure S1).

As it may be anticipated, H_A and H_B are weakly spin−spin coupled at 1.4 T, i.e., $^3J_{HA\text{-}HB}$ is ∼7 Hz, which is substantially smaller than their chemical shift difference of ∼0.5 ppm or 30 Hz. Therefore, each site undergoes relaxation on its own, and since the chemical nature of HP butane gas is the same regardless of the precursor identity (1-butene or 2-butene), monoexponential T_1 decay constants are anticipated to be the same. Indeed, T_1 values plotted as a function of pressure are effectively the same (within experimental error bars) for H_A protons, Figure 2c,f, respectively. For example, T_1 = 3.71 ± 0.03 s and T_1 = 3.81 ± 0.05 s for HP butane at 2.5 bar pressure, Figure 1b,e, respectively (see Table S1 for more details). However, the most important finding is that HP butane gas has significantly longer T_1 values than HP propane at all pressure values studied, Figure 2 and Table S1. For example, the HP butane H_A T_1 value (T_1 = 1.55 ± 0.05 s, Figure S2) is approximately 2.0 times longer than that of HP propane (T_1 = 0.79 ± 0.02 s, Figure S2) at 1 bar gas pressure, i.e., the pressure relevant in the context of biological applications (the presented HP propane T_1 relaxation results (Figure 2i) are in good agreement with previously reported values[48]). This fact of substantially longer T_1 in HP butane gas compared to that of the propane gas is crucial, because fast imaging sequences can allow multislice 2D or 3D MRI read-out in less than 1 s;[47] thus, the longer lifetime of the HP state provides a correspondingly longer time window for administration and imaging of HP gas on a time scale directly relevant to envisioned clinical applications. This increase in T_1 is rationalized through the decreased contribution by the spin-rotation relaxation mechanism due to the overall larger butane molecule size compared to propane.[50,51] Thus, HP butane clearly has a translational advantage over HP propane gas. The linear T_1 dependence on gas density (hence the gas pressure) is known for the relaxation of gases (including HP propane[48,49]) induced by the spin-rotation mechanism.[50,51] Additional T_1 measurements were taken for HP propane (produced from propene) and HP butane (produced from 1-butene) at 1 atm pressure by performing the experiment several times to confirm data reproducibility: these results are presented in Figure S2 and are also listed in Table S1.

Hyperpolarized Gas NMR Spectroscopy and T_S Relaxation Dynamics at 0.0475 T

When the magnetic field is sufficiently low (e.g., 0.0475 T), H_A and H_B are strongly spin−spin coupled; i.e., $^3J_{HA\text{-}HB}$ of ∼7 Hz is substantially greater than their chemical shift difference of only ∼1 Hz at this field. It has been previously shown that at such conditions long-lived spin states can exist in HP propane gas[60] and diethyl ether gas[53] produced via the process of p-H_2 pairwise addition with exponential decay constant T_S values that are 2−3 times longer than their corresponding T_1 values. Thus, low-field NMR experiments (e.g., 0.0475 T employed here) were performed with the rationale of creating LLSS and investigating the LLSS lifetime in the HP butane gas. It should be noted that, under these conditions, the NMR resonances of HP H_A and H_B protons created via p-H_2 pairwise addition should result in nearly complete signal cancellation.[60] To visualize otherwise NMR-silent LLSS, we have employed a partial SLIC pulse to partially convert LLSS into observable magnetization (for more details, please see ref 48), Scheme 2b. The resulting NMR spectrum exhibits a single resonance of coalesced H_A and H_B lines, Figure 3a (HP butane produced from 1-butene), Figure 3d (HP butane produced from 2-butene), and Figure 3g (HP propane). The application of partial SLIC pulses in a pseudo-2D fashion (Scheme 2b) also enabled monitoring the decay of LLSS for quantitative T_S measurements, Figure 3b,e,h, respectively. T_S exhibited a linear dependence on pressure for all HP gases studied, Figure 3c,f,i (the corresponding values for HP propane, Figure 3i, were in a good agreement with the previous study[48]). Overall, HP butanes (produced via p-H_2 addition either to 1-butene or 2-butene) exhibited significantly longer T_S values than those of HP propane at all pressure values studied: for example, T_S =

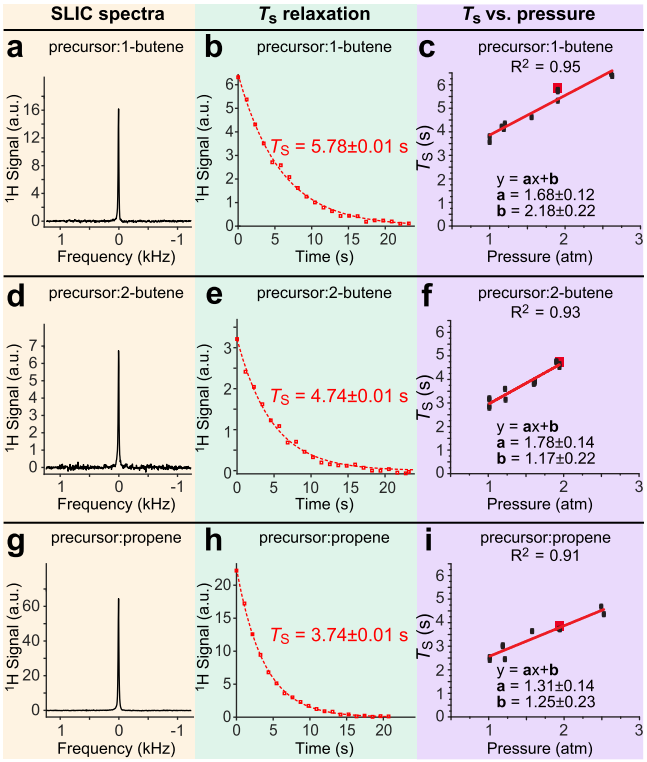

Figure 3. NMR spectroscopy, decay of LLSS, and T_S pressure dependence of HP butane and HP propane gases prepared via HET-PHIP and revealed via SLIC at 0.0475 T. (a) SLIC spectrum of HP butane prepared from 1-butene. (b) T_S relaxation decay of HP butane produced from 1-butene. (c) T_S pressure dependence of HP butane gas produced from 1-butene. (d) SLIC spectrum of HP butane prepared from 2-butene. (e) T_S relaxation decay of HP butane produced from 2-butene. (f) T_S pressure dependence of HP butane gas produced from 2-butene. (g) SLIC spectrum of HP propane produced from propene. (h) T_S relaxation decay of HP propane produced from propene. (i) T_S pressure dependence of HP propane gas produced from propene. Yellow, green, and purple color shading is used to guide the eye. The NMR spectra and decay plots are shown for pressure values denoted by the corresponding red squares in panels c, f, and i (the T_S error bars were relatively small (0.1 or less), and therefore, cannot be readily seen in those displays; see Table S2 for details).

https://doi.org/10.1021/cbmi.4c00041
Chem. Biomed. Imaging 2024, 2, 698−710

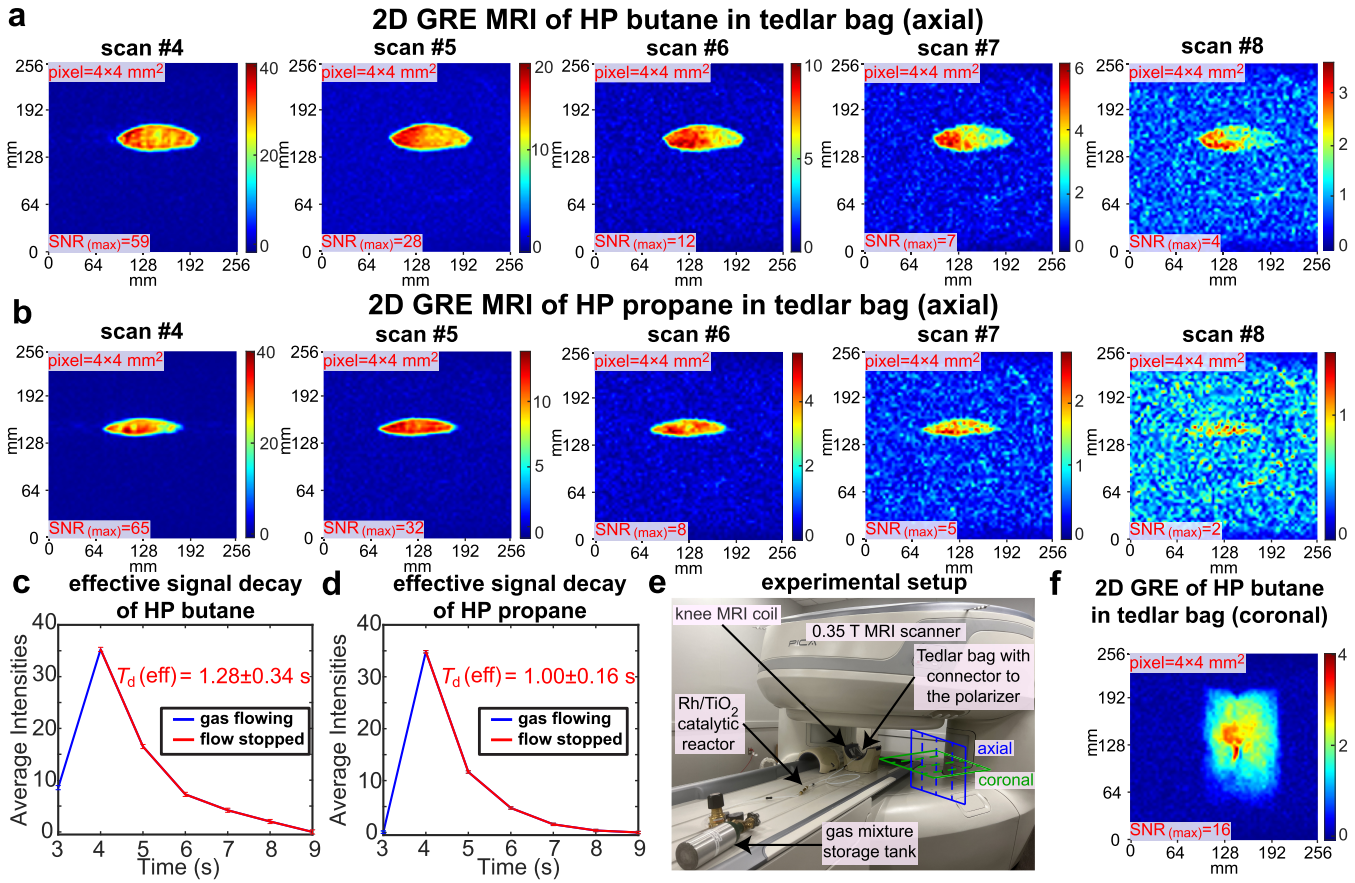

Figure 4. Phantom imaging studies of high-capacity HP butane and propane production using a 0.35 T clinical MRI scanner. (a) Time series of 2D MRI scans recorded on HP butane gas immediately after gas injection inside the Tedlar bag. The duration or temporal resolution of each back-to-back scan is 0.97 s. The $SNR_{(MAX)}$ values were obtained by selecting the highest intensity pixel from a 3 × 3 matrix in the highest intensity region and dividing it by RMS noise (obtained as an RMS value of signal intensities from the pixels from 3 × 3 matrix elements in the noise region). (b) Corresponding imaging time series obtained using HP propane gas. (c) Signal decay of HP butane gas over time (1 s roughly corresponds to 1 scan). The last 5 data points during the HP gas signal decay (when gas was definitely stopped) were used to measure the effective monoexponential signal decay constant T_d = 1.28 ± 0.34 s. (d) Corresponding effective signal decay of HP propane gas with effective T_d value of 1.00 ± 0.16 s. (e) Annotated photo of experimental setup showing the gas mixture storage tank, Rh/TiO_2 reactor, unmounted knee coil (axial and coronal planes indicated), and gas connection from the reactor outlet to the Tedlar bag (close-up photos are shown in Figures S6b and S10b). (f) Subsecond 2D GRE coronal image of HP butane injected in a Tedlar bag. All images were recorded with a 64 × 64 imaging matrix (converted to 256 × 256 in image post-processing) over 256 × 256 mm^2 FOV, 50 mm slice thickness, and 30° slice-selective RF pulse.

5.78 ± 0.01 s (Figure 3b), T_S = 4.74 ± 0.01 s (Figure 3e) versus HP propane T_S of 3.74 ± 0.01 s at the gas pressure of 1.9 bar, Table S2. While the overall T_S increase in HP butane versus HP propane gas (meaning the lifetime of LLSS became longer) was somewhat expected based on the T_1 pressure dependence discussed above, the substantial difference in T_S values for HP butane produced from 1-butene and 2-butene was somewhat unexpected. We rationalize this difference by the fact that different spin states may be overpopulated in the process of p-H_2 addition and polarization redistribution in the case of p-H_2 addition to 1-butene versus those spin states created via p-H_2 addition to *cis*- and *trans*-2-butene, Scheme 1. Since a different strongly coupled overpopulated spin ensemble may be created for each case, each one may undergo HP state decay with a unique T_S value that is different from other spin states created in otherwise chemically identical butane molecules. Relevant to the biomedical applications, T_S was 3.81 ± 0.03 s for HP butane produced from 1-butene, and T_S was 3.15 ± 0.05 s for HP butane produced form 2-butene at 1 bar gas pressure, Table S2. While both of these values were substantially longer than T_S of propane (2.54 ± 0.03 s), HP butane produced from 1-butene clearly exhibited the longest lifetime of LLSS. Therefore, the MRI studies reported below utilized 1-butene as a PHIP precursor for production of HP butane gas contrast agent.

High-Capacity Production of HP Butane Gas and Subsecond Imaging of Tedlar Bag Phantoms at 0.35 T

High-capacity production of HP propane and butane was accomplished using the modified setup shown in Figure 1b, allowing for a production speed of 30−40 sLm with the key rationale to deliver a clinically relevant bolus of HP butane or propane gas quickly (ideally in 1−2 s before substantial relaxation leads to gas depolarization) for future utility in imaging of pulmonary function in large animals and humans. NMR spectroscopic analysis of HP gas that was allowed to depolarize and gain thermal polarization at 1.4 T also revealed full chemical conversion and overall the same signal enhancement values as those obtained with a slower production rate of 6−8 sLm. Since only a small volume of gas was detected via NMR spectroscopy (~0.1 mL detection region) at 1.4 T, the produced HP gas (0.5−0.8 L batch produced in ~1 s) was injected in a one liter Tedlar bag with the rationale to confirm

https://doi.org/10.1021/cbmi.4c00041
Chem. Biomed. Imaging 2024, 2, 698−710

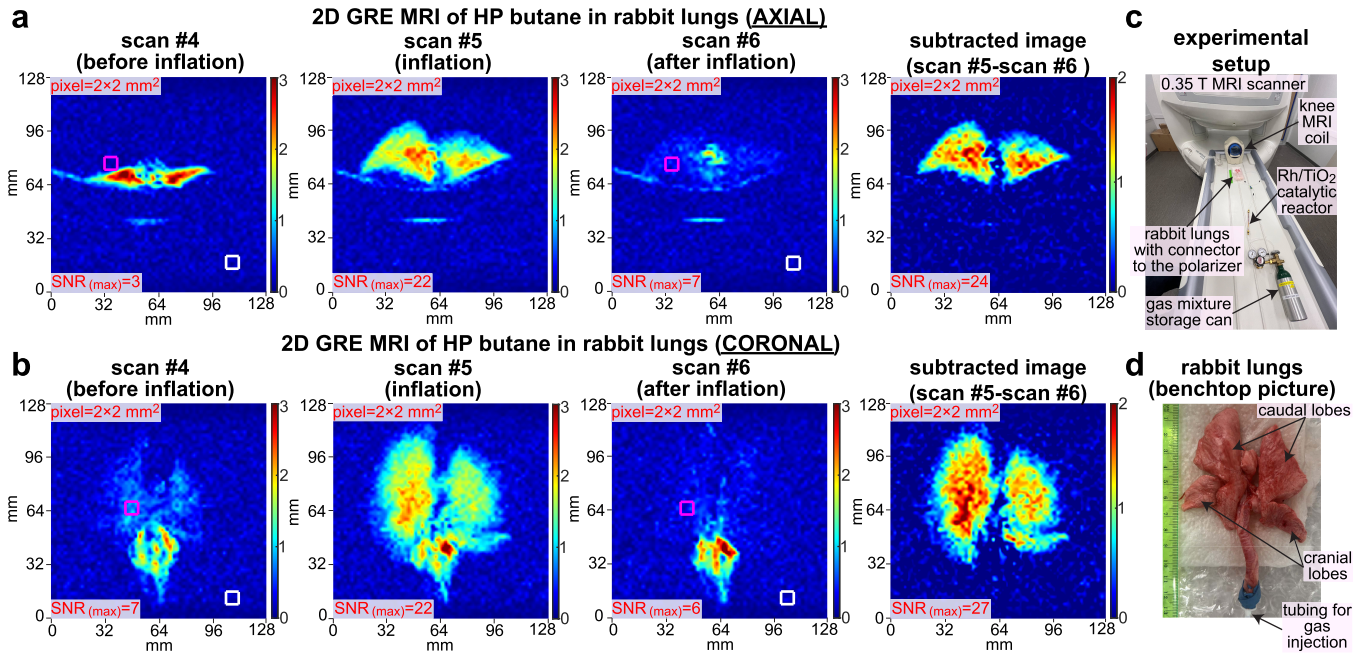

Figure 5. Subsecond 2D ventilation MRI using HP butane gas contrast agent injected in the excised rabbit lungs. (a) Time series of axial scans recorded before lungs' inflation with the HP butane (scan #4), at inflation (scan #5), after the inflation (scan #6), and the difference (or "subtracted") image obtained by subtracting the "scan #6" from "scan #5" image (to remove the background signals from surrounding tissues). The imaging parameters employed were the same as those used in Figure 4 except for the FOV that was reduced to 128 × 128 mm^2. (b) Corresponding time series recorded on a different HP butane gas injection in the same lungs in the coronal projection. (c) Annotated photo of experimental setup showing the gas mixture storage tank, Rh/TiO_2 reactor, 0.35 T knee MRI coil, and gas connection from the reactor outlet to the excised rabbit lungs. (d) Annotated photograph of the excised rabbit lungs used in the study.

that highly polarized gas was indeed created on a large scale. 2D GRE imaging of the HP butane or propane gas was performed on a Tedlar bag. HP butane (or propane) produced in the reactor filled the Tedlar bag within 1 s, and 2D images (set of 16 preprogrammed back-to-back repeat scans of 0.97 s each) were recorded on a bag before inflation, during inflation, and after the inflation was completed and HP gas was stopped. The first images of stopped HP butane (Figure 4a, scan #4) and HP propane (Figure 4b, scan #4) revealed relatively homogeneous signal intensities across the entire bag: note that the green pixels distributed at the edges are likely due to partial volume intensity loss. Once the gas was fully stopped, the image acquisition continued, and the resulting images (scans #5−8) exhibited the decrease of SNR (reported as the SNR of the highest-intensity pixel or $SNR_{(MAX)}$) due to the compounding effect of HP state relaxation and the effect of slice-selective excitation RF pulses of the imaging pulse sequence. To compute $SNR_{(MAX)}$, we have calculated the SNR of the highest-intensity pixels located in a 3 × 3 matrix selected from the brightest intensity region in the image of the inflated reservoir (Tedlar bag in Figure 4 or excised lungs in Figure 5) representing the maximum signal (examples of such $SNR_{(MAX)}$ calculations are shown in Figure S14) and a root-mean-square (RMS) intensity from nine elements of 3 × 3 matrix in the region far away from the signal to quantify the noise (example represented by the white colored box in Figure S14). Figure 4a,b shows the gradual decay in $SNR_{(MAX)}$: 59 → 28 → 12 → 7 → 4 for HP butane and 65 → 32 → 8 → 5 → 2 for HP propane, respectively, in five consecutively recorded MR images. We have also performed quantification of effective $SNR_{(MAX)}$ decay with time using monoexponential decay fitting function and reported it as a T_d to distinguish this signal decay constant from T_1 and T_S polarization decay. T_d(eff) of HP butane was found to be 1.28 ± 0.34 s (Figure 4c). This is longer than T_d(eff) of HP propane which was 1.00 ± 0.16 s (Figure 4d), albeit within the experimental error bars. This is in overall agreement with the spectroscopic studies—note that here the effects of the RF pulses are likely the dominant depolarization effect since T_d(eff) is smaller than the corresponding T_1 and T_S values for HP butane at 1 bar pressure.

MR imaging with both HP butane and HP propane was reproducible. Replication of HP butane and HP propane gas injection to the Tedlar bag and fast GRE sequence acquisition was run in axial (twice) and coronal (once) projections, and they revealed similar intensity distributions, $SNR_{(MAX)}$ values, and T_d(eff), Figures S6−S14. The excellent run-to-run MRI scan reproducibility confirms that high-capacity production of HP butane and HP propane gas contrast agents was also reproducible and the same HET-PHIP reactor setup can be recycled multiple times. The overall setup is shown in Figure 4e, with the close-up photo of the RF coil holding the inflated Tedlar bag shown in Figure S6b.

In addition to the axial projection scans, we have also performed HP butane and propane Tedlar bag imaging in coronal projection, Figures 4f, S10, and S13, albeit with lower $SNR_{(MAX)}$ values.

Pilot Ventilation Lung MRI Studies Employing HP Butane Using a Clinical 0.35 T MRI Scanner

Followed by successful phantom imaging studies, we performed lung ventilation imaging in excised rabbit lungs using HP butane gas as the contrast agent. Slight modification to the experimental setup shown in Figure 1b was made by changing the high-flow reactor manifold to the catalytic reactor setup employed for relaxation dynamics studies, providing an

https://doi.org/10.1021/cbmi.4c00041
Chem. Biomed. Imaging 2024, 2, 698−710

HP butane gas flow rate of ∼8 sLm that inflated the lungs in ∼1 s without causing structural damage (given the substantially smaller size of the rabbit lungs compared to the Tedlar bag phantom). We have employed the same overall approach for the ventilation imaging studies as that for the Tedlar bag imaging; i.e., the imaging sequence (consisting of 16 back-to-back repeat scans) was initiated before the HP gas inflation to ensure the inflation was captured correctly (of note, most MRI scanners have 2−4 s lag time between the time when the operator presses the "scan" button to the point of actual sequence execution). Figure 5a,b shows three representative scans (from the 16-scan series) with scan #4 recorded before HP gas inflation, scan #5 recorded at the time of lung inflation with HP butane gas, and scan #6 after the inflation in the axial and coronal projections. The MRI image in scan #4 shows only the signal originating from collapsed thermally polarized lung tissue (and other background signals), whereas scan #5 additionally contains the HP butane signal, clearly highlighting HP gas ventilation throughout the inflated lungs ($SNR_{(MAX)}$ = 22 for coronal and axial images). After the HP butane gas injection was completed, the lungs remained inflated, but very little HP gas signal was left: $SNR_{(MAX)}$ = 7, Figure 5a, scan #6. This observation is in line with the rapid signal decay of HP gas in the Tedlar bag phantoms (primarily due to the depolarizing effect of the excitation RF pulses), when the same sequence was employed as discussed above. More advanced pulse sequences can potentially address this limitation, for example, using faster scan speed and more efficient RF excitation pulsing.[64]

The key imaging artifact in the ventilation gas images is the proton background signal. However, a simple pixel-by-pixel image subtraction of scan #6 from scan #5 (Figure 5a,b) negates this challenge; indeed, a nearly perfect background suppression is seen in the subtracted images. The obtained ventilation images on clinical MRI equipment exhibit a remarkable spatial resolution of 2 × 2 mm^2 pixel size. Recording higher-resolution images is also feasible since the sensitivity of MRI is dependent on the available magnetization: Figure S14 demonstrates higher-resolution images with 1.6 × 1.6 mm^2 pixel size, albeit at the expense of SNR. However, it should be noted here that our experiments were not fully optimized: for example, the coil filling factor was unfavorable (small object in a large MRI coil), Figure 5c,d, and no ultrafast sequences were readily available. Moreover, the degree of polarization (estimated here at 0.5−1%) can also be substantially increased using more advanced and purpose-synthesized catalysts[42,65]—indeed, we hope that this work will stimulate the development of new materials for producing butane gas with a higher level of hyperpolarization. It should also be noted that, even at a nominally lower P level, HP butane detection sensitivity is similar or even better than that of the HP ^{129}Xe gas contrast agent. Indeed, a number of compounding fundamental advantages favor proton imaging: (i) γ_{129Xe} is only 27% of that of proton, (ii) each butane molecule carries two HP protons compared to monatomic xenon, and (iii) proton natural abundance is 1.2 times greater than that of 83% enriched ^{129}Xe. Therefore, it follows that HP butane with 1% polarization is equivalent to 33%-polarized enriched ^{129}Xe.[47] Furthermore, clinical MRI scanners naturally come with highly SNR-optimized detectors for proton imaging. We envision that the future use of optimized pulse sequences, compressed sensing,[64] and AI postprocessing[66] may drastically improve the quality and segmentation[67] of ventilation images using HP butane and other proton-hyperpolarized gas contrast agents. The key translational advantage of the presented technology is its robust production of HP gas media and utilization on a clinical MRI scanner for lung ventilation imaging, which is demonstrated here in the pilot report. At the same time, it should be made clear that, while ventilation imaging of HP butane has been demonstrated here and gas-phase diffusion imaging of HP butane can be potentially envisioned, HP butane will likely not be able to provide meaningful information about gas perfusion through the interstitial lung tissue and, therefore, would likely not be able to report on gas exchange in the lung. The key limiting reason is not the solubility of HP butane in the blood and lung tissue, but unlike Xe (exhibiting near 200 ppm difference between the gas and the dissolved phase), no substantial chemical shift difference is expected between the gas-phase and dissolved-phase HP butane NMR resonances, thus providing no spectroscopic mechanism to differentiate (and image) the two pools of HP contrast agent bolus.

Overall, HP butane gas has been successfully demonstrated to retain its HP state substantially longer than what is feasible with HP propane gas by exhibiting longer T_1 and T_S constants of HP state decay. This observation of longer lifetimes in HP butane is crucial for biomedical imaging applications using *proton*-hyperpolarized contrast media, as it provides a longer time window for administration and sensing of HP contrast agents. Pilot lung ventilation imaging studies performed here exhibit the potential use of HP butane as a low-cost, robust imaging contrast agent for pulmonary imaging and beyond.

As mentioned, butane is labeled as GRAS by the FDA—reflecting its low-toxicity profile. Butane is broadly employed in foods and other industries as an E943a additive. Indeed, a ninety-day randomized exposure study (10 000 ppm butane concentration) found no toxicologically important changes in parameters relating to systemic toxicity or neurotoxicity in rats.[68] Light anesthetic effects were observed in mice exposed to 220 000 ppm (or 22%) butane for 25 min.[69] The history of butane substance abuse in humans reports on butane primarily affecting central nervous system (CNS) and cardiac function.[70] In human volunteers, a 10 min exposure with 10 000 ppm butane yielded some drowsiness, but no irritation was noted up to 100 000 ppm (or 10%) butane concentration with exposure for a few minutes.[71] Based on the envisioned administration of an inhalation dose of 0.5−0.8 sL, it is anticipated that the intoxicating effect of a single dose will be substantially less than that of 10% butane/air for 1 min. The administration of multiple inhalations of HP butane gas at a lower dose may also be envisioned. However, it should be made clear that no current regulatory approval for the MRI applications of HP butane exists. Even though butane exhibits low toxicity, future HP butane pulmonary imaging scans would need to address adverse side effects potentially including cardiac and CNS depression.

Another potential approach to reduce the toxicity and flammability of HP butane gas contrast agent is to dilute the butene:p-H_2 reaction mixture or the produced HP gas with inert buffering gas, for example, using noble gases such as Ar or Kr: experiments in progress in our laboratories. Because the gas-phase T_1 and T_S (and by extension the lifetime of HP state) are limited by the spin rotation relaxation mechanism,[48,49] the addition of buffering gases with similar molecular weight (N_2, O_2, Ar, etc.) is anticipated to have no substantial effect of the relaxation dynamics. On the other hand, the

https://doi.org/10.1021/cbmi.4c00041
Chem. Biomed. Imaging 2024, 2, 698−710

addition of heavy buffering gas (e.g., Kr) may potentially pave the way to increasing the lifetime of the HP state. One should note, however, that the dilution leads to the decrease of the gas-phase concentration of the HP contrast agent and the corresponding reduction of NMR signal.

The lower explosivity limit (LEL) is 1.6%, and the upper explosivity limit (UEL) is 8.4% for butane gas according to the Center for Disease Control (CDC) and the Occupational Safety and Health Administration (OSHA). We envision the administration of HP butane as a single inhalable dose for *in vivo* applications (via a single inhalation) similarly to the well-documented use of hyperpolarized ^{129}Xe gas that is administered without mixing with oxygen (and thus preventing a potential formation of highly explosive mixtures in case of future administration of HP butane gas). Although a single dose (up to 1 L for the human scale) falls well below the LEL in any MRI suite (due to large room volume), we envision the exhaled butane gas to be captured by a carbon filter in a manner already established in routine anesthesiology practice (indeed, the exhaled gas anesthetics are readily captured by a carbon capturing filter on a scale ranging from small rodents all the way to human scale)—experiments are in progress in our partnering laboratories to validate this method of hydrocarbon gas capture by an activated carbon filter.

CONCLUSION

HP butane gas was successfully prepared by using two precursors (1-butene and 2-butene) via HET-PHIP hyperpolarization. During the process of hyperpolarization and transfer to the NMR detector, polarization redistribution likely occurs in the produced butane molecules resulting in creation of LLSS with distinctly different lifetimes. Remarkably, HP butane gas demonstrated substantially longer lifetimes of the gas-phase HP state compared to HP propane: for example, clinically relevant (1 bar pressure) exponential decay constants T_1 of 1.55 ± 0.05 s and T_S of 3.81 ± 0.03 s compare favorably to those of HP propane with T_1 of 0.79 ± 0.02 s and T_S of 2.54 ± 0.03 s, respectively. High-capacity production of HP butane gas with a production dose of 0.5−0.8 sL in 1 s has been demonstrated: the batch ejection was validated by subsecond 2D MR imaging at 0.35 T of Tedlar bag phantoms filled with HP gas. High-resolution ventilation imaging of HP butane gas was also successfully demonstrated by injecting a bolus of HP butane gas in excised rabbit lungs: subsecond images with up to 1.6 × 1.6 mm^2 in-plane resolution have been successfully recorded with a 0.35 T clinical MRI scanner using vendor-supplied sequences and hardware without any modification. The feasibility of low-field MRI using the HP butane contrast agent is also exciting for two crucial reasons: T_S is more than twice as long as T_1 for HP butane gas, enabling even longer time windows for contrast agent administration and scanning at low field compared to that at high magnetic field. At the same time, high-field clinical MRI scanners (e.g., 1.5 T, 3 T, and 7 T) are typically equipped with substantially faster gradients, therefore, enabling substantially faster scan speeds that are greatly desired for imaging of comparatively short-lived HP states: for example, a recent 3 T study demonstrated a scan speed of 0.4 s for acquiring 8 slices on HP propane gas in phantoms.[47] Moreover, the use of compressed sensing schemes may further substantially reduce the scan time. Therefore, even though the lifetime of the HP state is shorter at high field, the possibility of faster scan speeds may position clinical high-field MRI as a good imaging modality for pulmonary ventilation imaging in the future. Furthermore, bedside low-field MRI for brain imaging has been successfully introduced.[72] We envision that purpose-built MRI scanners for bedside functional pulmonary imaging may become possible when employing HP butane as an inhalable contrast agent, potentially providing tremendous value—especially for critically ill patients who cannot be readily transported to MRI or CT imaging suites. While future studies are certainly warranted to address the safety of HP butane inhalation, the pilot feasibility study reported here certainly bodes well for future *in vivo* use. The reported pilot results in phantoms and excised rabbit lungs serve as a good justification for near-future *in vivo* lung ventilation studies—work in progress in our partnering laboratories.

ASSOCIATED CONTENT

Supporting Information

The Supporting Information is available free of charge at https://pubs.acs.org/doi/10.1021/cbmi.4c00041.

Additional experimental details, tabulated relaxation data, reproducibility data and plots, T_1 and T_S relaxation studies in CD_3OD solvent, computations of signal enhancements, and image data processing details (PDF)

Examples of T_1 and T_S data processing using custom-made MATLAB code (ZIP)

AUTHOR INFORMATION

Corresponding Authors

Nuwandi M. Ariyasingha − *Department of Chemistry, Karmanos Cancer Institute (KCI), Integrative Biosciences (Ibio), Wayne State University, Detroit, Michigan 48202, United States*; Email: nuwandia@wayne.edu

Eduard Y. Chekmenev − *Department of Chemistry, Karmanos Cancer Institute (KCI), Integrative Biosciences (Ibio), Wayne State University, Detroit, Michigan 48202, United States*; orcid.org/0000-0002-8745-8801; Email: chekmenevlab@gmail.com

Authors

Anna Samoilenko − *Department of Chemistry, Karmanos Cancer Institute (KCI), Integrative Biosciences (Ibio), Wayne State University, Detroit, Michigan 48202, United States*

Md Raduanul H. Chowdhury − *Department of Chemistry, Karmanos Cancer Institute (KCI), Integrative Biosciences (Ibio), Wayne State University, Detroit, Michigan 48202, United States*

Shiraz Nantogma − *Department of Chemistry, Karmanos Cancer Institute (KCI), Integrative Biosciences (Ibio), Wayne State University, Detroit, Michigan 48202, United States*

Clementinah Oladun − *Department of Chemistry, Karmanos Cancer Institute (KCI), Integrative Biosciences (Ibio), Wayne State University, Detroit, Michigan 48202, United States*

Jonathan R. Birchall − *Department of Chemistry, Karmanos Cancer Institute (KCI), Integrative Biosciences (Ibio), Wayne State University, Detroit, Michigan 48202, United States*

Tarek Bawardi − *Department of Chemistry, Karmanos Cancer Institute (KCI), Integrative Biosciences (Ibio), Wayne State University, Detroit, Michigan 48202, United States*

Oleg G. Salnikov − *International Tomography Center SB RAS, Novosibirsk 630090, Russia*; orcid.org/0000-0003-2266-7335

Larisa M. Kovtunova − *International Tomography Center SB RAS, Novosibirsk 630090, Russia; Boreskov Institute of Catalysis SB RAS, Novosibirsk 630090, Russia*
Valerii I. Bukhtiyarov − *Boreskov Institute of Catalysis SB RAS, Novosibirsk 630090, Russia*
Zhongjie Shi − *Department of Pediatrics, Wayne State University, Detroit, Michigan 48202, United States*
Kehuan Luo − *Department of Pediatrics, Wayne State University, Detroit, Michigan 48202, United States*
Sidhartha Tan − *Department of Pediatrics, Wayne State University, Detroit, Michigan 48202, United States*
Igor V. Koptyug − *International Tomography Center SB RAS, Novosibirsk 630090, Russia;* orcid.org/0000-0003-3480-7649
Boyd M. Goodson − *School of Chemical & Biomolecular Sciences, Materials Technology Center, Southern Illinois University, Carbondale, Illinois 62901, United States;* orcid.org/0000-0001-6079-5077

Complete contact information is available at: https://pubs.acs.org/10.1021/cbmi.4c00041

Notes

The authors declare the following competing financial interest(s): E.Y.C. and B.M.G. declare a stake of ownership in XeUS Technologies LTD. E.Y.C. serves on the Scientific Advisory Board (SAB) and declares a stake of ownership in Vizma Life Sciences.

■ ACKNOWLEDGMENTS

This work was supported by DOD CDMRP W81XWH-20-10576, W81XWH-20-10578, NSF CHE-1905341 and CHE-1904780, NHLBI R21HL154032 and F32HL160108, R01NS114972, R01NS117146, and R01NS130258. I.V.K. and O.G.S. thank the Russian Science Foundation (Grant #22-43-04426) for financial support.

■ REFERENCES

(1) Eills, J.; Budker, D.; Cavagnero, S.; Chekmenev, E. Y.; Elliott, S. J.; Jannin, S.; Lesage, A.; Matysik, J.; Meersmann, T.; Prisner, T.; et al. Spin Hyperpolarization in Modern Magnetic Resonance. *Chem. Rev.* **2023**, *123* (4), 1417−1551.
(2) Hoult, D. I.; Richards, R. E. The signal-to-noise ratio of the nuclear magnetic resonance experiment. *J. Magn. Reson.* **1976**, *24* (1), 71−85.
(3) Goodson, B. M.; Whiting, N.; Coffey, A. M.; Nikolaou, P.; Shi, F.; Gust, B. M.; Gemeinhardt, M. E.; Shchepin, R. V.; Skinner, J. G.; Birchall, J. R.; et al. Hyperpolarization Methods for MRS. *Emagres* **2015**, *4* (4), 797−810.
(4) Nikolaou, P.; Goodson, B. M.; Chekmenev, E. Y. NMR Hyperpolarization Techniques for Biomedicine. *Chem.—Eur. J.* **2015**, *21* (8), 3156−3166.
(5) Kovtunov, K. V.; Pokochueva, E. V.; Salnikov, O. G.; Cousin, S.; Kurzbach, D.; Vuichoud, B.; Jannin, S.; Chekmenev, E. Y.; Goodson, B. M.; Barskiy, D. A.; et al. Hyperpolarized NMR: d-DNP, PHIP, and SABRE. *Chem.—Asian J.* **2018**, *13* (15), 1857−1871.
(6) Ardenkjaer-Larsen, J. H. On the present and future of dissolution-DNP. *J. Magn. Reson.* **2016**, *264*, 3−12.
(7) Reineri, F.; Cavallari, E.; Carrera, C.; Aime, S. Hydrogenative-PHIP polarized metabolites for biological studies. *Magn. Reson. Mater. Phys.* **2021**, *34*, 25−47.
(8) Barskiy, D. A.; Coffey, A. M.; Nikolaou, P.; Mikhaylov, D. M.; Goodson, B. M.; Branca, R. T.; Lu, G. J.; Shapiro, M. G.; Telkki, V.-V.; Zhivonitko, V. V.; et al. NMR Hyperpolarization Techniques of Gases. *Chem.—Eur. J.* **2017**, *23* (4), 725−751.
(9) Hövener, J.-B.; Pravdivtsev, A. N.; Kidd, B.; Bowers, C. R.; Glöggler, S.; Kovtunov, K. V.; Plaumann, M.; Katz-Brull, R.; Buckenmaier, K.; Jerschow, A.; et al. Parahydrogen-based Hyperpolarization for Biomedicine. *Angew. Chem., Int. Ed.* **2018**, *57* (35), 11140−11162.
(10) Golman, K.; Axelsson, O.; Johannesson, H.; Mansson, S.; Olofsson, C.; Petersson, J. S. Parahydrogen-induced polarization in imaging: Subsecond C-13 angiography. *Magn. Reson. Med.* **2001**, *46* (1), 1−5.
(11) Ardenkjaer-Larsen, J. H.; Fridlund, B.; Gram, A.; Hansson, G.; Hansson, L.; Lerche, M. H.; Servin, R.; Thaning, M.; Golman, K. Increase in signal-to-noise ratio of > 10,000 times in liquid-state NMR. *Proc. Natl. Acad. Sci. U. S. A.* **2003**, *100* (18), 10158−10163.
(12) Golman, K.; Ardenkjær-Larsen, J. H.; Petersson, J. S.; Månsson, S.; Leunbach, I. Molecular imaging with endogenous substances. *Proc. Natl. Acad. Sci. U. S. A.* **2003**, *100* (18), 10435−10439.
(13) Golman, K.; in't Zandt, R.; Thaning, M. Real-time metabolic imaging. *Proc. Natl. Acad. Sci. U. S. A.* **2006**, *103* (30), 11270−11275.
(14) Albert, M. S.; Cates, G. D.; Driehuys, B.; Happer, W.; Saam, B.; Springer, C. S.; Wishnia, A. Biological Magnetic-Resonance-Imaging Using Laser Polarized Xe-129. *Nature* **1994**, *370* (6486), 199−201.
(15) Mugler, J. P.; Altes, T. A. Hyperpolarized ^{129}Xe MRI of the human lung. *J. Magn. Reson. Imaging* **2013**, *37* (2), 313−331.
(16) Goodson, B. M. Nuclear magnetic resonance of laser-polarized noble gases in molecules, materials, and organisms. *J. Magn. Reson.* **2002**, *155* (2), 157−216.
(17) Khan, A. S.; Harvey, R. L.; Birchall, J. R.; Irwin, R. K.; Nikolaou, P.; Schrank, G.; Emami, K.; Dummer, A.; Barlow, M. J.; Goodson, B. M.; et al. Enabling Clinical Technologies for Hyperpolarized Xenon-129 MRI and Spectroscopy. *Angew. Chem., Int. Ed.* **2021**, *60* (41), 22126−22147.
(18) Driehuys, B.; Cates, G. D.; Miron, E.; Sauer, K.; Walter, D. K.; Happer, W. High-volume production of laser-polarized Xe-129. *Appl. Phys. Lett.* **1996**, *69* (12), 1668−1670.
(19) Walkup, L. L.; Woods, J. C. Translational applications of hyperpolarized ^{3}He and ^{129}Xe. *NMR Biomed.* **2014**, *27* (12), 1429−1438.
(20) Lilburn, D. M. L.; Pavlovskaya, G. E.; Meersmann, T. Perspectives of hyperpolarized noble gas MRI beyond ^{3}He. *J. Magn. Reson.* **2013**, *229*, 173−186.
(21) Walkup, L. L.; Thomen, R. P.; Akinyi, T. G.; Watters, E.; Ruppert, K.; Clancy, J. P.; Woods, J. C.; Cleveland, Z. I. Feasibility, tolerability and safety of pediatric hyperpolarized ^{129}Xe magnetic resonance imaging in healthy volunteers and children with cystic fibrosis. *Pediatr. Radiol.* **2016**, *46* (12), 1651−1662.
(22) Shih, W.-J.; Shih, G. L.; Milan, P. P. Xenon 133 Ventilation Studies as an Alternative for Detecting and Quantifying Fatty Infiltration of the Liver. *RadioGraphics* **2010**, *30* (4), 958−959.
(23) Muller, N. L.; Mayo, J. R.; Zwirewich, C. V. Value of MR imaging in the evaluation of chronic infiltrative lung diseases: comparison with CT. *Am. J. Roentgenol.* **1992**, *158* (6), 1205−1209.
(24) Mayo, J. R.; Mackay, A.; Muller, N. L. MR imaging of the lungs: value of short TE spin-echo pulse sequences. *Am. J. Roentgenol.* **1992**, *159* (5), 951−956.
(25) Ohno, Y.; Koyama, H.; Yoshikawa, T.; Matsumoto, K.; Takahashi, M.; VanCauteren, M.; Sugimura, K. T_2* measurements of 3-T MRI with ultrashort TEs: capabilities of pulmonary function assessment and clinical stage classification in smokers. *Am. J. Roentgenol.* **2011**, *197* (2), W279−W258.
(26) Salerno, M.; Altes, T. A.; Mugler, J. P.; Nakatsu, M.; Hatabu, H.; de Lange, E. E. Hyperpolarized noble gas MR imaging of the lung: potential clinical applications. *Eur. J. Radiol.* **2001**, *40*, 33−44.
(27) Moller, H. E.; Chen, X. J.; Saam, B.; Hagspiel, K. D.; Johnson, G. A.; Altes, T. A.; de Lange, E. E.; Kauczor, H.-U. MRI of the lungs using hyperpolarized noble gases. *Magn. Reson. Med.* **2002**, *47*, 1029−1051.
(28) van Beek, E. J.; Wild, J. M.; Kauczor, H. U.; Schreiber, W.; Mugler, J. P.; de Lange, E. E. Functional MRI of the lung using

hyperpolarized 3-helium gas. *J. Magn. Reson. Imaging* **2004**, *20*, 540−554.
(29) Matsuoka, S.; Patz, S.; Albert, M. S.; et al. Hyperpolarized gas MR imaging of the lung: current status as a research tool. *J. Thorac. Imaging* **2009**, *24*, 181−188.
(30) Fain, S.; Schiebler, M. L.; McCormack, D. G.; Parraga, G. Imaging of lung function using hyperpolarized helium-3 magnetic resonance imaging: review of current and emerging translational methods and applications. *J. Magn. Reson. Imaging* **2010**, *32*, 1398−1408.
(31) Witte, C.; Schroder, L. NMR of hyperpolarised probes. *NMR Biomed.* **2013**, *26* (7), 788−802.
(32) Shepelytskyi, Y.; Hane, F. T.; Grynko, V.; Li, T.; Hassan, A.; Albert, M. S. Hyperpolarized ^{129}Xe Time-of-Flight MR Imaging of Perfusion and Brain Function. *Diagnostics* **2020**, *10* (9), 630.
(33) Hane, F. T.; Li, T.; Smylie, P.; Pellizzari, R. M.; Plata, J. A.; DeBoef, B.; Albert, M. S. In vivo detection of cucurbit[6]uril, a hyperpolarized xenon contrast agent for a xenon magnetic resonance imaging biosensor. *Sci. Rep.* **2017**, *7*, 41027.
(34) Cleveland, Z. I.; Virgincar, R. S.; Qi, Y.; Robertson, S. H.; Degan, S.; Driehuys, B. 3D MRI of impaired hyperpolarized ^{129}Xe uptake in a rat model of pulmonary fibrosis. *NMR Biomed.* **2014**, *27* (12), 1502−1514.
(35) Driehuys, B. Crossing the Chasm(s): Demonstrating the Clinical Value of Hyperpolarized Gas MRI. *Acad. Radiol.* **2017**, *24* (1), 1−3.
(36) Driehuys, B.; Martinez-Jimenez, S.; Cleveland, Z. I.; Metz, G. M.; Beaver, D. M.; Nouls, J. C.; Kaushik, S. S.; Firszt, R.; Willis, C.; Kelly, K. T.; et al. Chronic Obstructive Pulmonary Disease: Safety and Tolerability of Hyperpolarized Xe-129 MR Imaging in Healthy Volunteers and Patients. *Radiology* **2012**, *262* (1), 279−289.
(37) Walker, T. G.; Happer, W. Spin-exchange optical pumping of noble-gas nuclei. *Rev. Mod. Phys.* **1997**, *69* (2), 629−642.
(38) Eisenschmid, T. C.; Kirss, R. U.; Deutsch, P. P.; Hommeltoft, S. I.; Eisenberg, R.; Bargon, J.; Lawler, R. G.; Balch, A. L. Para Hydrogen Induced Polarization In Hydrogenation Reactions. *J. Am. Chem. Soc.* **1987**, *109* (26), 8089−8091.
(39) Bowers, C. R.; Weitekamp, D. P. Transformation of Symmetrization Order to Nuclear-Spin Magnetization by Chemical-Reaction and Nuclear-Magnetic-Resonance. *Phys. Rev. Lett.* **1986**, *57* (21), 2645−2648.
(40) Koptyug, I. V.; Kovtunov, K. V.; Burt, S. R.; Anwar, M. S.; Hilty, C.; Han, S. I.; Pines, A.; Sagdeev, R. Z. Para-hydrogen-induced polarization in heterogeneous hydrogenation reactions. *J. Am. Chem. Soc.* **2007**, *129* (17), 5580−5586.
(41) Kovtunov, K. V.; Zhivonitko, V. V.; Skovpin, I. V.; Barskiy, D. A.; Koptyug, I. V. Parahydrogen-induced polarization in heterogeneous catalytic processes. *Top. Curr. Chem.* **2012**, *338*, 123−180.
(42) Zhao, E. W.; Maligal-Ganesh, R.; Xiao, C.; Goh, T.-W.; Qi, Z.; Pei, Y.; Hagelin-Weaver, H. E.; Huang, W.; Bowers, C. R. Silica-Encapsulated Pt-Sn Intermetallic Nanoparticles: A Robust Catalytic Platform for Parahydrogen-Induced Polarization of Gases and Liquids. *Angew. Chem., Int. Ed.* **2017**, *56* (14), 3925−3929.
(43) Bouchard, L. S.; Kovtunov, K. V.; Burt, S. R.; Anwar, M. S.; Koptyug, I. V.; Sagdeev, R. Z.; Pines, A. Para-hydrogen-enhanced hyperpolarized gas-phase magnetic resonance imaging. *Angew. Chem., Int. Ed.* **2007**, *46* (22), 4064−4068.
(44) Kovtunov, K. V.; Barskiy, D. A.; Coffey, A. M.; Truong, M. L.; Salnikov, O. G.; Khudorozhkov, A. K.; Inozemtseva, E. A.; Prosvirin, I. P.; Bukhtiyarov, V. I.; Waddell, K. W.; et al. High-resolution 3D Proton Hyperpolarized Gas MRI Enabled by Parahydrogen and Rh/TiO_2 Heterogeneous Catalyst. *Chem.—Eur. J.* **2014**, *20* (37), 11636−11639.
(45) Salnikov, O. G.; Nikolaou, P.; Ariyasingha, N. M.; Kovtunov, K. V.; Koptyug, I. V.; Chekmenev, E. Y. Clinical-Scale Batch-Mode Production of Hyperpolarized Propane Gas for MRI. *Anal. Chem.* **2019**, *91* (7), 4741−4746.
(46) Schmidt, A. B.; Bowers, C. R.; Buckenmaier, K.; Chekmenev, E. Y.; de Maissin, H.; Eills, J.; Ellermann, F.; Glöggler, S.; Gordon, J. W.; Knecht, S.; et al. Instrumentation for Hydrogenative Parahydrogen-Based Hyperpolarization Techniques. *Anal. Chem.* **2022**, *94* (1), 479−502.
(47) Ariyasingha, N. M.; Samoilenko, A.; Birchall, J. R.; Chowdhury, M. R. H.; Salnikov, O. G.; Kovtunova, L. M.; Bukhtiyarov, V. I.; Zhu, D. C.; Qian, C.; Bradley, M.; et al. Ultra-Low-Cost Disposable Hand-Held Clinical-Scale Propane Gas Hyperpolarizer for Pulmonary Magnetic Resonance Imaging Sensing. *ACS Sens.* **2023**, *8* (10), 3845−3854.
(48) Ariyasingha, N. M.; Salnikov, O. G.; Kovtunov, K. V.; Kovtunova, L. M.; Bukhtiyarov, V. I.; Goodson, B. M.; Rosen, M. S.; Koptyug, I. V.; Gelovani, J. G.; Chekmenev, E. Y. Relaxation Dynamics of Nuclear Long-Lived Spin States in Propane and Propane-d6 Hyperpolarized by Parahydrogen. *J. Phys. Chem. C* **2019**, *123* (18), 11734−11744.
(49) Barskiy, D. A.; Salnikov, O. G.; Romanov, A. S.; Feldman, M. A.; Coffey, A. M.; Kovtunov, K. V.; Koptyug, I. V.; Chekmenev, E. Y. NMR Spin-Lock Induced Crossing (SLIC) Dispersion and Long-Lived Spin States of Gaseous Propane at Low Magnetic Field (0.05 T). *J. Magn. Reson.* **2017**, *276*, 78−85.
(50) Lemaire, C.; Armstrong, R. L. Proton spin longitudinal relaxation time in gaseous ammonia and hydrogen chloride. *J. Chem. Phys.* **1984**, *81* (4), 1626−1631.
(51) True, N. S. Gas Phase Applications of NMR Spectroscopy. In *Encyclopedia of Spectroscopy and Spectrometry*; Lindon, J. C., Ed.; Elsevier: Oxford, 1999; pp 660−667.
(52) Ariyasingha, N. M.; Chowdhury, M. R. H.; Samoilenko, A.; Salnikov, O. G.; Chukanov, N. V.; Kovtunova, L. M.; Bukhtiyarov, V. I.; Shi, Z.; Luo, K.; Tan, S.; et al. Toward Lung Ventilation Imaging Using Hyperpolarized Diethyl Ether Gas Contrast Agent. *Chem.—Eur. J.* **2024**, *30* (25), No. e202304071.
(53) Ariyasingha, N. M.; Joalland, B.; Younes, H. R.; Salnikov, O. G.; Chukanov, N. V.; Kovtunov, K. V.; Kovtunova, L. M.; Bukhtiyarov, V. I.; Koptyug, I. V.; Gelovani, J. G.; et al. Parahydrogen-Induced Polarization of Diethyl Ether Anesthetic. *Chem.—Eur. J.* **2020**, *26*, 13621−13626.
(54) Pravica, M. G.; Weitekamp, D. P. Net NMR Alighnment By Adiabatic Transport of Parahydrogen Addition Products To High Magnetic Field. *Chem. Phys. Lett.* **1988**, *145* (4), 255−258.
(55) Ariyasingha, N. M.; Nantogma, S.; Samoilenko, A.; Salnikov, O. G.; Chukanov, N. V.; Kovtunova, L. M.; Koptyug, I. V.; Chekmenev, E. Y. Efficient polarization redistribution in hyperpolarized 1-D-propane produced via pairwise parahydrogen addition. *J. Magn. Reson. Open* **2023**, *16*−*17*, No. 100135.
(56) Nantogma, S.; Joalland, B.; Wilkens, K.; Chekmenev, E. Y. Clinical-Scale Production of Nearly Pure (>98.5%) Parahydrogen and Quantification by Benchtop NMR Spectroscopy. *Anal. Chem.* **2021**, *93* (7), 3594−3601.
(57) Barskiy, D. A.; Kovtunov, K. V.; Gerasimov, E. Y.; Phipps, M. A.; Salnikov, O. G.; Coffey, A. M.; Kovtunova, L. M.; Prosvirin, I. P.; Bukhtiyarov, V. I.; Koptyug, I. V.; et al. 2D Mapping of NMR Signal Enhancement and Relaxation for Heterogeneously Hyperpolarized Propane Gas. *J. Phys. Chem. C* **2017**, *121* (18), 10038−10046.
(58) Coffey, A. M.; Truong, M. L.; Chekmenev, E. Y. Low-field MRI can be more sensitive than high-field MRI. *J. Magn. Reson.* **2013**, *237*, 169−174.
(59) DeVience, S. J.; Walsworth, R. L.; Rosen, M. S. Preparation of Nuclear Spin Singlet States Using Spin-Lock Induced Crossing. *Phys. Rev. Lett.* **2013**, *111* (17), 173002-1−173002-5.
(60) Kovtunov, K. V.; Truong, M. L.; Barskiy, D. A.; Koptyug, I. V.; Coffey, A. M.; Waddell, K. W.; Chekmenev, E. Y. Long-lived Spin States for Low-field Hyperpolarized Gas MRI. *Chem.—Eur. J.* **2014**, *20* (45), 14629−14632.
(61) Vasquez-Vivar, J.; Shi, Z.; Luo, K.; Thirugnanam, K.; Tan, S. Tetrahydrobiopterin in antenatal brain hypoxia-ischemia-induced motor impairments and cerebral palsy. *Redox Biol.* **2017**, *13*, 594−599.
(62) Vasquez-Vivar, J.; Shi, Z.; Jeong, J.-W.; Luo, K.; Sharma, A.; Thirugnanam, K.; Tan, S. Neuronal vulnerability to fetal hypoxia-

https://doi.org/10.1021/cbmi.4c00041
Chem. Biomed. Imaging 2024, 2, 698−710

reoxygenation injury and motor deficit development relies on regional brain tetrahydrobiopterin levels. *Redox Biol.* **2020**, *29*, 101407.
(63) Shi, Z.; Luo, K.; Jani, S.; February, M.; Fernandes, N.; Venkatesh, N.; Sharif, N.; Tan, S. Mimicking partial to total placental insufficiency in a rabbit model of cerebral palsy. *J. Neurosci. Res.* **2022**, *100* (12), 2138−2153.
(64) Milshteyn, E.; von Morze, C.; Reed, G. D.; Shang, H.; Shin, P. J.; Larson, P. E. Z.; Vigneron, D. B. Using a local low rank plus sparse reconstruction to accelerate dynamic hyperpolarized ^{13}C imaging using the bSSFP sequence. *J. Magn. Reson.* **2018**, *290*, 46−59.
(65) Gyton, M. R.; Royle, C. G.; Beaumont, S. K.; Duckett, S. B.; Weller, A. S. Mechanistic Insights into Molecular Crystalline Organometallic Heterogeneous Catalysis through Parahydrogen-Based Nuclear Magnetic Resonance Studies. *J. Am. Chem. Soc.* **2023**, *145* (4), 2619−2629.
(66) Iglesias, J. E.; Schleicher, R.; Laguna, S.; Billot, B.; Schaefer, P.; McKaig, B.; Goldstein, J. N.; Sheth, K. N.; Rosen, M. S.; Kimberly, W. T. Quantitative Brain Morphometry of Portable Low-Field-Strength MRI Using Super-Resolution Machine Learning. *Radiology* **2023**, *306* (3), No. e220522.
(67) Koonjoo, N.; Zhu, B.; Bagnall, G. C.; Bhutto, D.; Rosen, M. S. Boosting the signal-to-noise of low-field MRI with deep learning image reconstruction. *Sci. Rep.* **2021**, *11* (1), 8248.
(68) McKee, R. H.; Herron, D.; Saperstein, M.; Podhasky, P.; Hoffman, G. M.; Roberts, L. The Toxicological Properties of Petroleum Gases. *Int. J. Toxicol.* **2014**, *33*, 28S−51S.
(69) Stoughton, R. W.; Lamson, P. D. The relative anaesthetic activity of the butanes and pentanes. *J. Pharmacol. Exp. Ther.* **1936**, *58*, 175−177.
(70) Vahabzadeh, M.; Mégarbane, B. A two-decade review of butane toxicity as a substance of abuse. *Basic Clin. Pharmacol. Toxicol.* **2022**, *131* (3), 155−164.
(71) Patty, F. A.; Yant, W. P. *Odor Intensity and Symptoms Produced by Commercial Propane, Butane, Pentane, Hexane, and Heptane Vapor*; U.S. Department of Commerce, Bureau of Mines: Washington, DC, 1929.
(72) Yuen, M. M.; Prabhat, A. M.; Mazurek, M. H.; Chavva, I. R.; Crawford, A.; Cahn, B. A.; Beekman, R.; Kim, J. A.; Gobeske, K. T.; Petersen, N. H.; et al. Portable, low-field magnetic resonance imaging enables highly accessible and dynamic bedside evaluation of ischemic stroke. *Sci. Adv.* **2022**, *8* (16), eabm3952.

https://doi.org/10.1021/cbmi.4c00041
Chem. Biomed. Imaging 2024, 2, 698−710